Anharmonic Quasiclassical Barrier Samplings in Trajectory Calculations and Their Influence on the Computed Product Energy Distributions

Emilio Martínez-Núñez and Saulo A. Vázquez*

Departamento de Química Física, Universidad de Santiago de Compostela, Santiago de Compostela E-15706, Spain

Received: November 22, 2000; In Final Form: February 26, 2001

Harmonic and anharmonic quasiclassical barrier samplings were used in classical dynamics simulations to evaluate product energy distributions (PEDs). The results obtained for the CH dissociation in the methanethiol cation ($CH_3SH^+ \rightarrow CH_2SH^+ + H$) show that the PEDs are changed under inclusion of anharmonicity in the initial conditions. Both the vibrational energy content at the transition state and the energy in the transitional modes are important to explain the differences found in the PEDs. Discrepancies between the PEDs obtained for trajectories initiated at the barrier and those initiated at the reactant were found and explained on the basis of dynamical phase space bottlenecks, which make the phase space density not uniform for $t \neq 0$.

Introduction

The analysis of product energy distributions (PEDs) is one of the basic topics in the study of unimolecular reactions. Their measurement is often more readily accomplished than the measurement of the dissociation rate, and as a result, there exists a considerable body of experimental information about PEDs. From the theoretical side, PEDs can be calculated from statistical or nonstatistical models.[1] For reactions occurring with a potential energy barrier, the statistical redistribution of the product energies is often not possible even though the energy distribution at the barrier may be statistical. In these cases, the products rapidly dissociate with considerable translational energy and having little chance to randomize the available energy. Consequently, several nonstatistical models, for example, the impulsive model[2,3] and the transition state mapping model,[4−7] or classical trajectories are frequently used to obtain PEDs for reactions with a (tight) transition state. Classical trajectories are problematic because the inaccurate treatment of the zero-point energy (ZPE) may lead to inaccurate PEDs. However, with an initiation of the trajectories at the barrier with the quasiclassical model,[8] the unphysical ZPE leakage may not be a serious problem.

Recently, Hase and co-workers[9,10] designed an algorithm to obtain a quasiclassical microcanonical sampling of the vibrational states at the barrier (here called QCBS). Their approach gives the quasiclassical analogue of the quantum harmonic RRKM distribution. This means that all harmonic vibrational levels with energy less than the available energy (the total energy minus the barrier height) have equal probability of selection. Inclusion of anharmonicity could substantially modify both the reaction coordinate and the vibrational state distributions at the barrier and, consequently, the computed PEDs. Song et al.[11] proposed a semiclassical model for calculating anharmonic energy levels along the reaction path, which could be applied to barrier sampling.

In the present paper, we analyze the effect of using anharmonic initial conditions on the computed PEDs by studying the CH bond dissociation of the methanethiol cation ($CH_3SH^+ \rightarrow CH_2SH^+ + H$), which has a barrier height of 56 kcal/mol and a reaction endothermicity of 54.3 kcal/mol.[12] This system was selected because we have recently developed an analytical potential energy surface (PES) for it and obtained an anharmonic correction factor for the reactant and transition state densities of states.[11] In this study, this anharmonic correction together with the QCBS algorithm are used to construct various anharmonic quasiclassical barrier sampling models. The PEDs obtained with these anharmonic models are analyzed and compared with those obtained with the harmonic QCBS one. Finally, we also compared the PEDs obtained from trajectories initiated at the barrier with those obtained from trajectories initiated at the reactant phase space with an appropriate statistical sampling.

Methods

A. Harmonic Quasiclassical Barrier Sampling (QCBS) Model. The harmonic QCBS procedure[9,10] is based on the corresponding method for classical barrier sampling.[13] In the quasiclassical model, each harmonic vibrational level with energy less than the available energy E_{av} has equal probability of being selected and, therefore, the reaction coordinate and vibrational state distributions are in agreement with quantum harmonic RRKM theory. Hereinafter, the total available energy at the transition state (E_{av}) will be 169.4 kcal/mol with respect to the transition state ZPE (or 171.5 with respect to the product ZPE).

In this quasiclassical model, the initial conditions of each trajectory are selected as follows. A normal mode i is picked up at random and assigned n_i quanta by using an appropriate weighting. More precisely, the probability of assigning n_i quanta to a normal mode is given by[9,10]

$$P(n_i) = \frac{W_{n_i}}{W_{tot}} \tag{1}$$

where W_{tot} is the total number of harmonic states with energy less than E_{av} and W_{n_i} is the number of harmonic states with energy less than E_{av} and with mode i having n_i quanta. Both

* To whom correspondence should be addressed. Fax: 34 981 595012. E-mail: qfsaulo@usc.es.

10.1021/jp004267w CCC: $20.00
Published on Web 04/26/2001

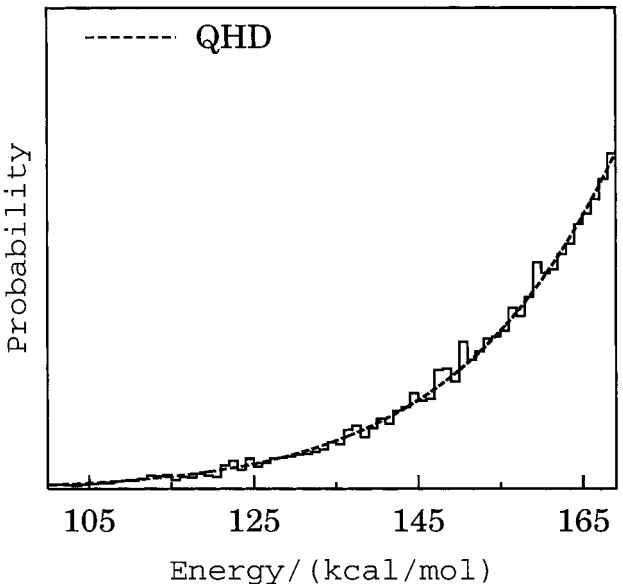

Figure 1. Normalized vibrational state distribution at the transition state obtained with the QCBS algorithm. The QHD is also shown for comparison. Note that the energies in this case are referred to the transition state ZPE.

W_{n_i} and W_{tot} were calculated by the Beyer−Swinehart algorithm.[14] Once n_i quanta have been assigned to mode i, the remaining energy, $E_{av} - E_i$, is distributed among the other modes in a similar manner. Hence, a second mode l is randomly chosen and assigned n_l quanta such that $E_l \leq E_{av} - E_i$. The probability of assigning n_l quanta to this mode follows the above equation, but in this case, W_{tot} is the total number of states considering only the remaining modes with energy less than $E_{av} - E_i$ and accordingly for W_{n_i}.

After all normal modes (m) have been assigned quanta (n_1, n_2, ..., n_m), the remaining energy $E_{av} - \sum_{i=1}^{m} E_i$ is placed on the reaction coordinate. Finally, the Cartesian coordinates and momenta are obtained from the displacement of the normal modes from the equilibrium at the transition state.[15] This model was used to prepare an ensemble of 10 000 trajectories at the barrier.

The quantum harmonic distribution (QHD) probability of vibrational levels is given by

$$P(E) = \rho(E)/W(E_{av}) \tag{2}$$

where $\rho(E)$ is the transition state harmonic density of states at energy E and $W(E_{av})$ is the total harmonic number of states with energy less than E_{av}, which acts in eq 2 as a normalization factor. Figure 1 shows the normalized vibrational state distribution obtained for 10 000 points sampled with the QCBS procedure as described above and the QHD (dashed line) obtained from eq 2. Both curves show a very good agreement as expected.

B. Anharmonic Corrections. The QHD can be substantially modified under inclusion of anharmonicity, as shown later. For the CH bond dissociation in the methanethiol cation, we have recently obtained an anharmonic correction factor for the density and sum of states.[12] This factor was calculated by fitting anharmonic RRK models to microcanonical rate constants, following previous work by Song and Hase.[16] The model used in ref 12 multiplies the harmonic RRK expression

$$k(E) = \nu(1 - E_0/E)^{s-1} \tag{3}$$

by the classical anharmonic factor[16]

$$f_{anh}^{cl}(E) = \frac{\exp(b^{ts}(E - E_0))}{\exp(bE)(1 + bE/s)} \tag{4}$$

where ν, b, and b^{ts} (with ts standing for transition state) are adjustable parameters, s is the number of vibrational degrees of freedom, and E_0 is the classical barrier height. The numerator and denominator in eq 4 give the classical correction factor for the transition state sum of states and for the reactant density of states, respectively. It is important to stress the empirical character of the anharmonic correction factor used here. This correction factor is usually a reasonable approximation but is not guaranteed to be adequate for every system.[16] Using the above equations to fit the microcanonical rate constants for the $CH_3SH^+ \rightarrow CH_2SH^+ + H$ reaction, we obtained a value of 0.054 for b^{ts},[12] which can be used to determine the classical anharmonic density of states at the transition state as

$$\rho_{anh}^{cl}(E) = \rho_{harmonic}^{cl}(E) \exp(b^{ts}E)(1 + b^{ts}E/s) \tag{5}$$

Now, to obtain a quantum anharmonic distribution, we need a quantum anharmonic correction factor, which can be evaluated from the classical anharmonic one as[17]

$$f_{anh}^{q}(E) = f_{anh}^{cl}(E - (1 - a)E_{zpe}) \tag{6}$$

where an appropriate fraction of the ZPE E_{zpe} is subtracted from the classical energy E, following the Whitten-Rabinovitch approximation.[18] The parameter a is a function of energy and is determined by equating the harmonic quantum and classical densities of states, that is

$$\rho_{harmonic}^{q}(E) = \rho_{harmonic}^{cl}(E - (1 - a)E_{zpe}) \tag{7}$$

where a must be unity in the classical limit (high energies) and zero for low energies. Particularly, we have chosen $a = \tanh(a_0 E^{a_1})$ and adjusted a_0 and a_1 until good agreement between both members of eq 7 was achieved; the final values of a_0 and a_1 were 0.77 and 0.20, respectively. Then, the quantum anharmonic density of states can be determined from the classical one as[17]

$$\rho_{anh}^{q}(E) = \rho_{anh}^{cl}(E - (1 - a)E_{zpe}) \tag{8}$$

Now, introducing the quantum anharmonic density of states and the quantum anharmonic sum of states $W_{anh}^{q}(E_{av}) = \int_0^{E_{av}} \rho_{anh}^{q}(E)\, dE$ into eq 2, one obtains the quantum anharmonic RRKM distribution (QAD) of vibrational states depicted in Figure 2. As seen in the figure, the QHD (dashed line) and QAD (solid line) differ substantially. The reaction coordinate energy distribution (not shown for simplicity) is analogously modified by inclusion of anharmonicity.

C. Anharmonic Sampling Models. To obtain a QAD from the QCBS method, one may consider, as a first approximation, a collection of uncoupled Morse oscillators for which the energy of a given oscillator is

$$E = \left(n + \frac{1}{2}\right)hc\tilde{\nu}_e - \left(n + \frac{1}{2}\right)^2 \chi_e hc\tilde{\nu}_e \tag{9}$$

where n is the quantum number, χ_e is the anharmonic constant, and $\tilde{\nu}_e$ is the vibrational wavenumber. Therefore, by using the Stein-Rabinovitch algorithm[19] to compute the density and sum of states, a quantum Morse-oscillator RRKM distribution (QMOD) of the vibrational levels can be obtained. Table 1 shows the vibrational wavenumbers for the transition state and

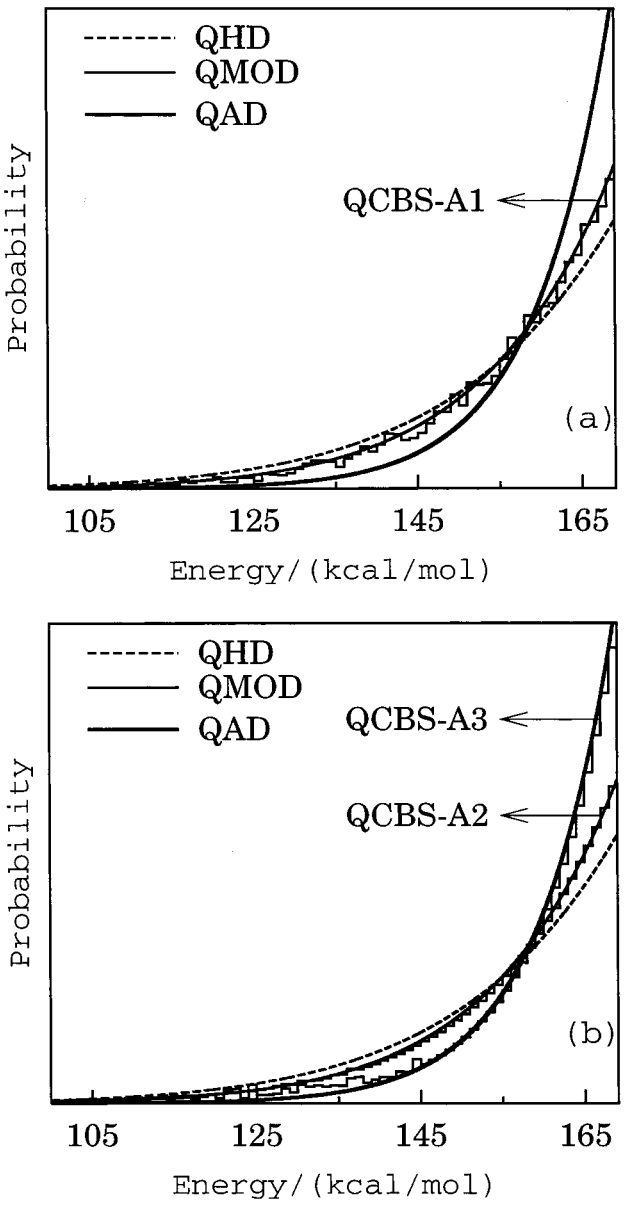

Figure 2. Normalized vibrational state distributions at the transition state obtained for the (a) QCBS-A1 and (b) QCBS-A2 and QCBS−A3 algorithms (depicted as histograms). The QAD, QHD, and QMOD are shown for comparison in both panels. Note that the energies in this case are referred to the transition state ZPE.

the corresponding anharmonic constants χ_e for the CS, SH, and CH_2 stretching normal modes, evaluated as $\chi_e = hc\tilde{\nu}_e/4D_e$ (with the dissociation energies D_e taken from ref 12). The QMOD obtained with this simple model (not shown for simplicity) differs strongly from the QAD obtained in the previous section. To improve the agreement between the QMOD and the QAD, the anharmonic constant χ_e of each normal mode was modified; the third column of Table 1 collects the new χ_e values. However, even in this case the QMOD distribution still differs substantially from the QAD as shown in Figure 2. To a certain extent, the disagreement between the QMOD and the QAD distributions comes from the fact that the latter takes into account not only the anharmonicity but also the vibrational coupling. However, there may be a more fundamental problem with the QMOD. Attempts have been made in the past by Haarhoff[20] and Troe[21] to evaluate anharmonic molecular sums and densities of states with Morse oscillator-based Hamiltonians, and a major difficulty arose from the fact that bend and torsions were not necessarily well represented by Morse oscillators. Therefore, the same limitation may apply here.

TABLE 1: Vibrational Wavenumbers and Anharmonic Constants for the Transition State

		χ_e	
mode	vibrational wavenumber	from ref 12[a]	QCBS-A1
1	327 (HCS bend)		0.003 058
2	362 (torsion)		0.005 525
3	812 (CSH bend)		0.009 852
4	994 (CH_2/SH wagg)		0.013 078
5	1009 (CS stretch)	0.016 811	0.012 884
6	1256 (CH_2 rock)		0.014 331
7	1336 (CH_2 wagg)		0.014 970
8	1745 (CH_2 scissors)		0.015 473
9	2552 (SH stretch)	0.022 520	0.039 969
10	3360 (CH_2 stretch)	0.044 475	0.047 619
11	3486 (CH_2 stretch)	0.046 143	0.047 619

[a] Calculated as $\chi_e = hc\tilde{V}/4D_e$ with the frequencies and dissociation energies taken from ref 12 (see text).

Even though the QMOD cannot reproduce the QAD, an anharmonic QCBS model based on uncoupled Morse oscillators was designed following the steps detailed previously for the QCBS model, but in this case, eq 1 was evaluated by considering the 11 uncoupled Morse oscillators described in Table 1 (column 3) and using the Stein−Rabinovitch algorithm.[19] This modified QCBS model was called here QCBS-A1 and when 10 000 points were sampled in this way we obtained the normalized distribution depicted in Figure 2a.

We propose two other anharmonic samplings (QCBS-A2 and QCBS-A3) designed from the harmonic QCBS scheme. Both samplings, which comprise 10 000 sampling points, include a subset of points selected with constraints in order to obtain an anharmonic distribution of vibrational levels at the barrier. More specifically, in the QCBS-A2 model, the first 7000 points were selected with the standard QCBS procedure and the remaining 3000 points were chosen with the constraint that the root-mean-square (rms) deviation between the normalized QCBS-A2 distribution and the QMOD decreased progressively as every new point was considered. Therefore, both the QCBS-A2 and QCBS-A1 models match the QMOD as shown in Figure 2 (panels a and b). On the other hand, in the QCBS-A3 model, the last 5000 points were selected with a constraint to progressively reduce the rms deviation between the normalized QCBS-A3 distribution and the QAD (see Figure 2b). Basically, this procedure implies to populate high-energy vibrational levels by depleting low-energy states from the harmonic normalized distribution.

Figure 3 shows the initial average normal mode energies obtained in the four barrier samplings. As can be seen, the QCBS, QCBS-A2, and QCBS-A3 ensembles predict a similar behavior for the normal mode energy distribution: the normal mode energies decrease as the vibrational wavenumber increases. However, the normal mode energy partitioning for QCBS-A1 is substantially different. Particularly, modes 9−11 (SH stretch and the two CH_2 stretches) have more energy in the QCBS-A1 model than in the others. This is easily understood by the strong decrease in the vibrational energy of the SH (or CH_2) stretch by inclusion of anharmonicity for a given quantum number, allowing more vibrational levels to be populated. By contrast, the initial energy content for mode 1 (HCS bend) is smaller for QCBS-A1.

D. Trajectory Computational Details. The trajectory calculations, performed with the GenDyn code[22] and using the analytical PES described in ref 12, were initialized in five ways.

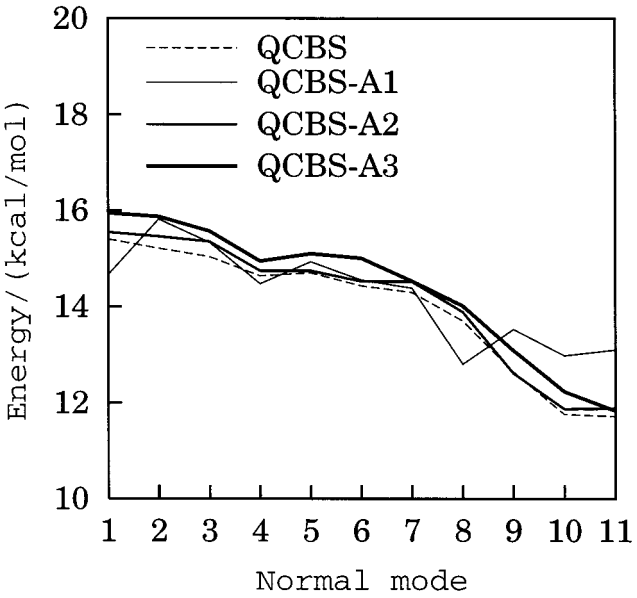

Figure 3. Average normal mode vibrational energies at the transition state for the QCBS, QCBS-A1, QCBS-A2, and QCBS-A3 models.

TABLE 2: PEDs[a] (in kcal/mol) Obtained for the QCBS Ensembles

	ensemble			
	QCBS	QCBS-A1	QCBS-A2	QCBS-A3
$<E_{trans}>$	33.9 ± 17.4	31.1 ± 16.2	32.5 ± 17.2	30.7 ± 16.5
$<E_{vib}>$	128.7 ± 21.4	131.5 ± 20.2	130.2 ± 21.0	131.8 ± 20.6
$<E_{rot}>$	8.9 ± 7.9	8.9 ± 7.7	8.8 ± 7.8	9.0 ± 8.0

[a] Energies are referred to the CH_2SH^+ ZPE (24.14 kcal/mol). Listed uncertainties are the standard deviations of the distributions.

Four of them correspond to the QCBS, QCBS-A1, QCBS-A2, and QCBS-A3 models as described above. The fifth is the efficient microcanonical sampling (EMS)[23,24] with $J = 0$, which takes into account the anharmonicity and vibrational coupling of the PES. For details of the EMS initial conditions the reader is referred to our previous trajectory study.[12] The energy for the EMS-initialized trajectories was 220.4 kcal/mol above the reactant ZPE, which corresponds to 169.4 kcal/mol at the transition state. Hereinafter, the names EMS, QCBS, QCBS-A1, QCBS-A2, and QCBS-A3 will be also used to name the ensembles associated to the different samplings.

Batches of 10 000 trajectories were integrated for a maximum of 5 ps or until dissociation occurred (more specifically, until one of the CH interatomic distances exceeded 10 Å). When a trajectory finished, a final product analysis was performed from the atomic Cartesian coordinates and momenta.[25,26]

Results

Table 2 collects the average PEDs obtained in this work for the QCBS models and Figure 4 shows the product translational energy distributions obtained from the QCBS, QCBS-A1, and QCBS-A3 ensembles. As seen from the figure and the table, there are discrepancies between the results obtained from the harmonic and anharmonic samplings, pointing out that anharmonicity may be important in barrier sampling initial conditions. Particularly, the anharmonic models predict lower translational energies and higher vibrational energies than the harmonic QCBS. To a large extent, this is a result of the marked differences between the average reaction coordinate energies (and therefore between the average vibrational energies, too) at the transition state, as shown in Table 3. In general, an anharmonic correction to quasiclassical barrier sampling is expected to become important at high total energies and for reactions where there is a small potential energy release in the exit channel. Both of these are the case for the reaction that is being studied here. At low total energies, however, the harmonic sampling model becomes more accurate. In addition, for reactions with a large potential energy release, which may be

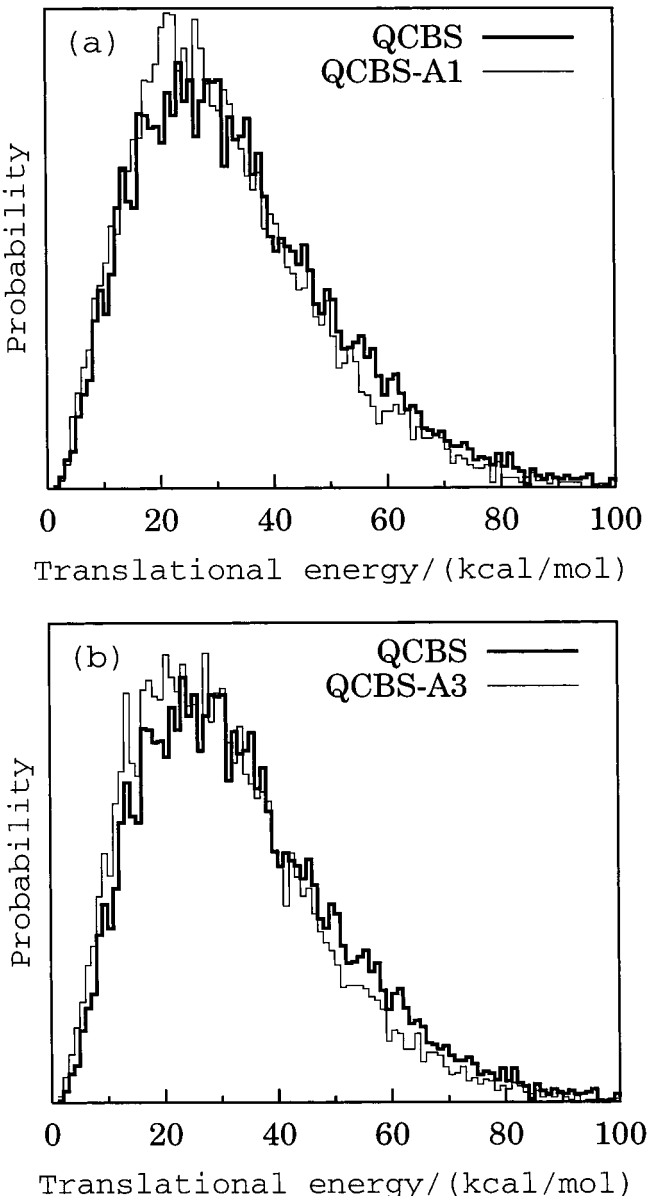

Figure 4. Normalized translational energy distributions obtained for the (a and b) QCBS, (a) the QCBS-A1, and (b) the QCBS-A3 ensembles.

TABLE 3: Average Vibrational Normal Mode and Reaction Coordinate Energies[a] at the Transition State for the QCBS Ensembles

	average energies at the transition state			
	QCBS	QCBS-A1	QCBS-A2	QCBS-A3
$<E_{dis}>^b$	30.6 ± 6.8	30.5 ± 6.5	30.8 ± 6.7	31.9 ± 6.7
$<E_{vib}>^c$	153.5 ± 14.5	156.5 ± 12.5	155.1 ± 14.1	158.1 ± 12.6
$<E_{rc}>^d$	15.9 ± 14.5	12.9 ± 12.5	14.3 ± 14.1	11.3 ± 12.6

[a] Energies are in kcal/mol and referred to the transition state ZPE. Listed uncertainties are the standard deviations of the distributions. [b] Average energy in disappearing modes 1 and 2. [c] Average of the total vibrational energy. [d] Average reaction coordinate energy.

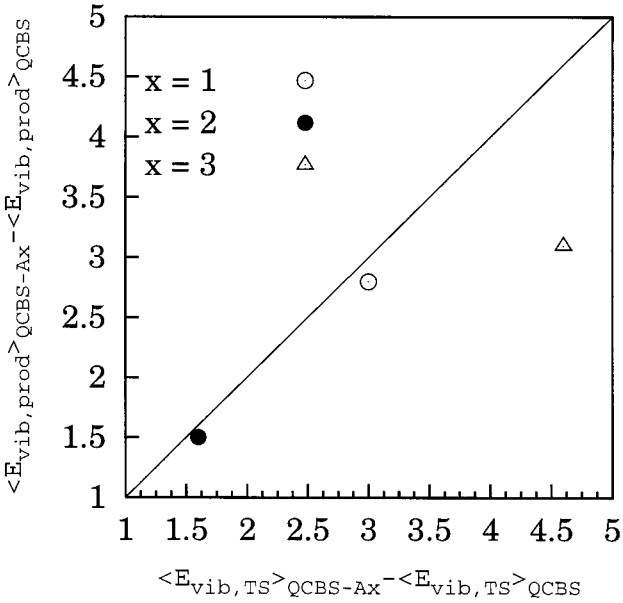

Figure 5. Differences (in kcal/mol) between the average vibrational energies for QCBS-Ax ($x = 1$ open circle, $x = 2$ solid circle, and $x = 3$ triangle) and QCBS, evaluated at the transition state (x axis) and at the product (y axis).

larger than the excess energy at the barrier, this energy release may dominate the product energy partitioning. As a result, the anharmonic correction to the sampling may be unimportant. The effect of anharmonicity on the PEDs has been studied for aluminum cluster dissociation, a reaction without an exit-channel barrier.[27]

The calculations predict that the difference between the average vibrational energies obtained by the anharmonic and harmonic models ($<E_{vib}>_{QCBS-Ax} - <E_{vib}>_{QCBS}$, with $x = 1$, 2, or 3) is almost conserved on going from the transition state to products, except for QCBS-A3, as illustrated in Figure 5. The lack of correlation for the QCBS-A3 ensemble may be explained by arguments based on the statistical adiabatic channel model (SACM).[1,21,28,29] In this model, the reactive system is assumed to remain in the same vibrational/rotational quantum level as it evolves along the reaction path. If the vibrational/rotational energy level spacings are similar at the barrier and for the products, all of the barrier classical potential energy goes to product translation. If the energy level spacings decrease in going from the barrier to products, energy transfer to product translation can be enhanced. In our case, two "transitional" or "disappearing" modes (the HCS bend and the torsion) correlate to product rotations. Because in these modes the vibrational levels are more widely spaced than the product rotational levels, a portion of the energy is expected to go to product translation. As shown in Table 3, the initial energy in these modes is almost the same for QCBS, QCBS-A1, and QCBS-A2. The corresponding energy for QCBS-A3 is somewhat higher, particularly, 1.4 kcal/mol higher than that for QCBS. Therefore, one may expect for QCBS-A3 an extra loss of total vibrational energy in going from the transition state to products as compared with the other ensembles (see Figure 5), and, concomitantly, a slight increase in the product rotational energy.

We have also computed the PEDs for an ensemble with anharmonic initial conditions at the reactant (EMS ensemble); the results are shown in Table 4 (last column). As can be seen, there are large discrepancies between the average PEDs obtained for the EMS and QCBS ensembles. The PEDs calculated for the EMS ensemble are in better agreement with the anharmonic

TABLE 4: PEDs[a] (in kcal/mol) Obtained for the EMS Ensembles

	ensemble		
	EMS1	EMS2	EMS
$<E_{trans}>$	34.2	30.3	27.8
$<E_{vib}>$	132.6	136.6	139.0
$<E_{rot}>$	4.7	4.6	4.7

[a] Energies are referred to the CH_2SH^+ ZPE (24.14 kcal/mol).

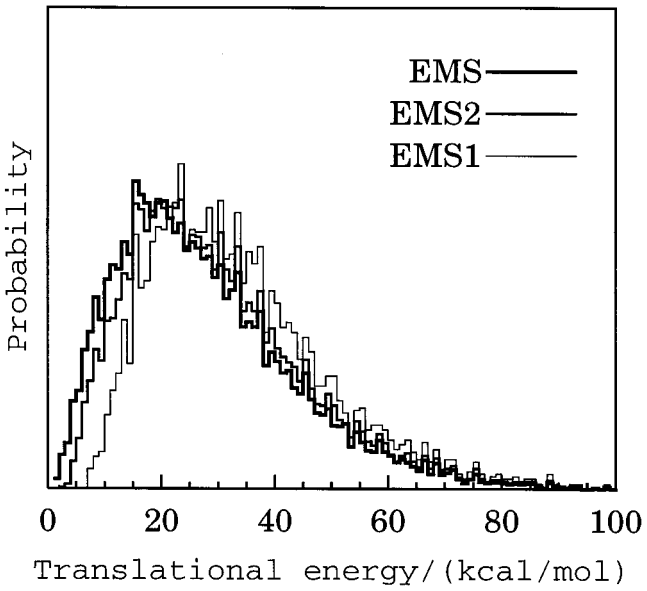

Figure 6. Normalized translational energy distributions obtained for the EMS, EMS2, and EMS1 ensembles.

than with the harmonic PEDs (obtained from barrier samplings). At first glance, one is tempted to suggest that this is a result of including anharmonicity in the barrier sampling. However, as concluded below, the better agreement with the anharmonic PEDs is rather fortuitous. One has to take into account the fact that the ZPE leakage may affect the EMS ensemble more strongly, so that the translational energy for this ensemble is expected to be higher than for the QCBS ensembles. This contrasts with the results obtained in this study (28 kcal/mol for EMS vs 31−34 kcal/mol for the QCBS ensembles). We found similar "striking" results for the dissociation of the propionyl radical[30] and the HF elimination of fluorethene.[31] As suggested in our previous study,[31] this unexpected trend may be a result of intrinsic non-RRKM behavior in the EMS-initialized trajectories. In other words, the EMS ensemble may be no longer microcanonical for $t \neq 0$ because of the presence of dynamical phase space bottlenecks, which keep the vibrational energy trapped. As a consequence, the transition state vibrational energy distribution may differ markedly from the statistical (RRKM or QCBS) one. To illustrate the above statement, we designed two new ensembles from the EMS one: EMS1, which comprises the first 4000 trajectories that dissociate, and EMS2, which comprises the first 7000. As shown in Figure 6, the translational energy distributions shift to lower energies as one goes from EMS1 to EMS. The EMS ensemble contains more phase space points associated to intramolecular bottlenecks than does the EMS1 ensemble. Consequently, the resulting vibrational energy content in the CH_2SH^+ product is larger because for more trajectories the energy remains trapped into a small subset of modes. One would expect that in the limit $t \rightarrow 0$ the PEDs obtained from the EMS ensemble will compare better with the QCBS results. However, there are still severe discrep-

ancies, mainly for the rotational energy content of CH_2SH^+, which is approximately twice for the QCBS ensemble. To a large extent, these discrepancies are a result of the classical nature of the EMS model. In other words, the vibrational and reaction coordinate energy distributions in the EMS ensemble at the transition state for $t \approx 0$ follows the classical but not the quantum vibrational distributions (imposed in the QCBS models). Therefore, a more rigorous comparison (between results of trajectories initiated in the reactant region with EMS and those of trajectories initiated at the barrier) would involve the use of the classical barrier sampling at the transition state rather than the quasiclassical barrier sampling.

Concluding Remarks

In the present work, the effects of including anharmonicity in barrier sampling initial conditions were analyzed. For this purpose, the PEDs obtained for the CH bond cleavage in the methanethiol cation were compared for various harmonic and anharmonic models. One anharmonic model is based on a collection of uncoupled Morse oscillators, and in the others, the vibrational level distributions at the barrier are artificially constructed from the harmonic QCBS model. Anharmonicity in the initial conditions alters the reaction coordinate energy and vibrational state distributions and, consequently, the PEDs. The energy content in two transitional modes (HCS bend and torsion) is found to be almost the same for all of the QCBS models, except for QCBS-A3. This explains that for this anharmonic model there is no correlation between the average vibrational energy at the barrier and that at the products.

The comparison between the PEDs obtained from barrier samplings and those initiated with the EMS algorithm shows that large deviations arise from the inherent non-RRKM behavior of the system at the selected energy.

Finally, we conclude that for systems with high anharmonicity (e.g., H−C−C, Al_3, Ar_{14}, HCN, H_2CO, and H−C≡C−H [ref 1, and references therein]) one may expect substantial discrepancies between the PEDs obtained from harmonic and anharmonic excitation schemes. By knowing in detail the anharmonicity of the transition state vibrational levels, however, one can calculate more realistic PEDs from one of the QCBS models proposed here and therefore make a more detailed comparison with the experiment (if available).

Acknowledgment. We are pleased to acknowledge financial support from MEC (BQU2000-0462). We also thank "Centro de Supercomputación de Galicia" CESGA for the use of their computational devices.

References and Notes

(1) Baer, T.; Hase, W. L. *Unimolecular Reaction Dynamics: Theory and Experiments*; Oxford University Press: New York, 1996.
(2) Holdy, K. E.; Klotz, L. C.; Wilson, K. R. *J. Chem. Phys.* **1970**, *52*, 4588.
(3) Busch, G. E.; Wilson, K. R.; *J. Chem. Phys.* **1972**, *56*, 3626.
(4) Qian, C. X. W.; Ogai, A.; Iwata, L.; Reisler, H. *J. Chem. Phys.* **1990**, *92*, 4296.
(5) Ogai, A.; Brandon, J.; Reisler, H.; Suter, H. U.; Huber, J. R.; von Dirke, M.; Schinke, R.; *J. Chem. Phys.* **1992**, *96*, 6643.
(6) Solter, D.; Werner, H. J.; von Dirke, M.; Untch, A.; Vegiri, A.; Schinke, R. *J. Chem. Phys.* **1992**, *97*, 3357.
(7) Reisler, H.; Keller, H. M.; Schinke, R. *Comments At. Mol. Phys.* **1994**, *30*, 191.
(8) Thrular, D. G.; Muckerman, J. T. *Atom-Molecule Collision Theory*; Bernstein, R. B., Ed.; Plenum Press: New York, 1979; pp. 505−566.
(9) Doubleday, C., Jr.; Bolton, K.; Peslherbe, G. H.; Hase, W. L. *J. Am. Chem. Soc.* **1996**, *118*, 9922.
(10) Bolton, K.; Hase, W. L.; Doubleday, C., Jr. *Ber. Bunsen-Ges. Phys. Chem.* **1997**, *3*, 414.
(11) Song, K.; Peslherbe, G. H.; Hase, W. L.; Dobbyn, A. J.; Stumpf, M.; Schinke, R. *J. Chem. Phys.* **1995**, *103*, 8891.
(12) Martínez-Núñez, E.; Vázquez, S. A. *J. Phys. Chem. A* **1999**, *103*, 9783.
(13) Hase, W. L.; Buckowski, D. G. *Chem. Phys. Lett.* **1980**, *74*, 284.
(14) Gilbert, R. G.; Smith, S. C. *Theory of Unimolecular and Recombination Reactions*; Blackwell Scientific Publications: Oxford, U.K., 1990.
(15) Sloane, C. S.; Hase, W. L. *J. Chem. Phys.* **1977**, *66*, 1523.
(16) Song, K.; Hase, W. L. *J. Chem. Phys.* **1999**, *110*, 6198.
(17) Peslherbe, G. H.; Hase, W. L. *J. Chem. Phys.* **1996**, *105*, 7432 and references therein.
(18) Tardy, D. C.; Rabinovitch, B. S.; Whitten, G. Z. *J. Chem. Phys.* **1965**, *48*, 1427.
(19) Stein, S. E.; Rabinovitch, B. S. *J. Chem. Phys.* **1973**, *58*, 2438.
(20) Haarhoff, P. C. *Mol. Phys.* **1963**, *6*, 337; **1963**, 7, 101.
(21) Troe, J. *J. Chem. Phys.* **1983**, *79*, 6017.
(22) Thompson, D. L. GenDyn program.
(23) Schranz, H. W.; Nordholm, S.; Nyman, G. *J. Chem. Phys.* **1991**, *94*, 1487.
(24) Nyman, G.; Nordholm, S.; Schranz, H. W. *J. Chem. Phys.* **1990**, *93*, 6767.
(25) Bunker, D. L. *Methods Comput. Phys.* **1971**, *10*, 287 and references therein.
(26) Raff, L. M.; Thompson, D. L. *Theory of Chemical Reaction Dynamics*; M. Baer CRC: Boca Raton, FL, 1985.
(27) Peslherbe, G. H.; Hase, W. L. *J. Phys. Chem.* **2000**, *104*, 10556.
(28) Quack, M.; Troe, J. *Ber. Bunsen-Ges. Phys. Chem.* **1974**, *78*, 240.
(29) Quack, M.; Troe, J. *Int. Rev. Phys. Chem.* **1981**, *1*, 97.
(30) Martínez-Núñez, E.; Peña-Gallego, A.; Vázquez, S. A. *J. Chem. Phys.* **2001**, *114*, 3546.
(31) Martínez-Núñez, E.; Vázquez, S. A. *Chem. Phys. Lett.* **2000**, *332*, 583.